CFD *Letters*   **www.cfdl.issres.net**   Vol. 1 (1) – July 2009

Numerical Investigation of Incompressible Flow Past Circular Tubes in Confined Channel

S. Jayavel[1] and Shaligram Tiwari[1c]
[1]*Department of Mechanical Engineering*
Indian Institute of Technology Madras, INDIA

Abstract

A three-dimensional computational code has been developed for the investigation of unsteady laminar flow past single and two inline circular tubes cross-confined in a channel. The developed code is based on the SIMPLE algorithm using finite volume technique to solve the governing equations. A body-fitted, multi-block structured grid has been generated for discretization of the incompressible form of conservation equations of mass, momentum and energy. The computational results correspond to a fixed Reynolds number of 400 based on tube diameter. The instantaneous flow and heat transfer characteristics for single and two inline tubes have been compared using streamline plots, temperature contours, vorticity contours, span-averaged pressure and span-averaged Nusselt number.

Keywords: Body-fitted grid; non-staggered variables; Channel confinement; unsteady channel flow; circular tubes.

1.   Introduction

The circular cylinder is a common bluff body and forms a large separated stagnant wake. The characteristics of separated wakes cannot be predicted analytically and hence must be analyzed either numerically or experimentally. Unlike square or rectangular cylinders, where the flow separates from the leading edges, the flow separation may occur from any location of a circular cylinder, further complicating the analysis. The difficulties in predicting flow and heat transfer around circular cylinders get multiplied when two or more of these cylinders are placed in proximity to each other and confined between channel walls. The large separated wakes behind each of the cylinders interact with each other and with the horseshoe vortices to give rise to a flow that is characteristically much more different than the flow past a single cylinder. Tiwari *et al.* [1] studied unsteady flow past confined circular tube and observed that the onset of vortex shedding gets delayed due to the effect of channel confinement. Patil and Tiwari [2] have carried out two-dimensional numerical investigations to study the behaviour of unsteady wake for flow past an inline arrangement of square cylinders confined in a channel. They studied the influence of the relative size and arrangement of the two inline cylinders on vortex shedding characteristics in their wakes. In engineering applications complex turbulent flows commonly occur. Wilson and

Bassiouny [3] predicted the pressure drop and heat transfer characteristics of laminar and turbulent flow of air across tube bundles (single and two rows), where the tube surfaces are maintained at constant temperature. Baker [4] studied the oscillatory behaviour of vortices formed at a single tube-plate junction in the transitional regime, between the steady laminar horseshoe vortices formed at low Re and the fully turbulent horseshoe vortices that occur at higher Re values. He reported that vortex oscillations begin at $Re_D = 1000$, and break down into full turbulence at $Re_D = 1600$. Roychowdhury et al. [5] studied numerically the effect of Re and tube spacing on flow and heat transfer over staggered tube banks. They observed that both the Re and tube spacing influence the vortex formation and growth in the region between the tubes. For sufficiently small spacing, eddy formation gets completely suppressed even at higher Reynolds number. Nishimura *et al.* [6] studied flow characteristics past tube banks in staggered as well as inline arrangement in the transitional flow regime at intermediate Reynolds numbers ($50 \leq Re_D \leq 1000$), where the flow is steady at the entrance of the tube banks, but becomes oscillatory downstream beyond a location of onset of vortex shedding. They found that the location of onset of vortex shedding moves upstream with increasing Re, and the upstream development of flow transition are much faster for the staggered array of tubes than for the in-line array. Much work has been devoted to these kinds of flows with vortex shedding. Williamson [7] has given a review for unbounded flow past a circular cylinder, and Zdravkovich [8] provides a lot of information on flow past circular cylinders.

In the present study, flow past single and two inline arrangement of tubes has been considered with wall confinement, which mimics the fin-tube heat exchanger geometry corresponding to tubes of finite length bounded by two fins as shown in Figure 1. A three-dimensional numerical study on the flow and heat transfer characteristics in a narrow confined flow with built-in inline circular tubes in cross-flow has been carried out to study the unsteady characteristics of the flow and heat transfer. The computations are carried out using finite volume based three-dimensional computational developed code corresponding to a $Re_D = 400$ in presence of channel confinement where the flow is expected to be laminar as confirmed by [1]. Several reports on solution algorithm and analysis of finite volume method are available from studies of Ju and Du [9], Piller and Stalio [10], Lacor *et al.* [11] and Pereira *et al.* [12].

2. Problem definition

The computational domain for flow past circular tubes, cross-confined and built-in with a rectangular channel is shown in Figure 1 with all dimensions shown in terms of channel height. All the length scales have been non-dimensionalized with respect to channel height, *H*. The channel is designed to mimic a passage formed by any two neighbouring fins in a fin-tube heat exchanger.

$l_1 = 20H, \quad l_2 = 10H, \quad l_{c1} = 5H, \quad l_{c2} = 10H$

where, $H = l_3$
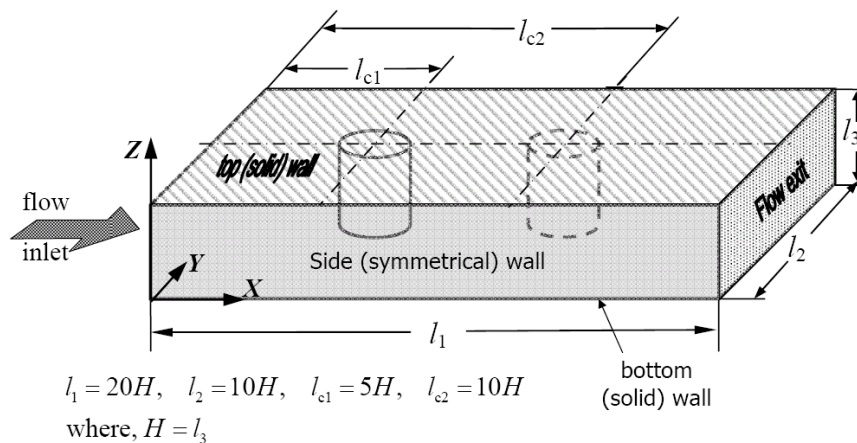
Figure 1. Computational domain

3.   Numerical details
3.1. Governing equations

The Navier-Stokes equations for the laminar flow in an arbitrary domain of volume *V* bounded by a closed surface **S** can be expressed in the following general convection-diffusion-source integral form:

$$\frac{\partial}{\partial t}\int_V \rho \, dV + \int_S \rho \mathbf{u} \cdot d\mathbf{S} = 0 \tag{1}$$

$$\frac{\partial}{\partial t}\int_V \rho \phi \, dV + \int_S [\rho \mathbf{u}\phi] \cdot d\mathbf{S} = \int_S [\Gamma_\phi \nabla \phi] \cdot d\mathbf{S} + \int_V S_\phi \, dV \tag{2}$$

where ϕ is the general transport variable , by setting ϕ equal to 1, *u, v, w* and *T* and selecting appropriate values for the diffusion coefficient Γ and source terms, the equations for mass, momentum and energy conservation are obtained. The diffusion coefficient, Γ_ϕ for example, represents viscosity. In Eqn. (2) the first term on the left hand side signifies the rate of change of the total accumulation of transport property ϕ in the control volume. The second term in left hand side, $\rho \mathbf{u}\phi$ expresses the convection flux component of the transport property ϕ due to the fluid flow along the outward face normal vector. Therefore, the net rate of change of fluid property ϕ for the fluid element due to convection is indicated by the second term on the left hand side of Eqn. (2). The first term on the right hand side represents the net rate of increase of property ϕ of the fluid element due to diffusion and the last term known as volumetric source term gives the rate of increase of property ϕ due to sources present inside the fluid element.

3.2. Discretization of Governing Equations:

Finite volume method on a non-staggered grid has been employed in the present study. The method is implemented directly on complex physical domain, where all dependent variables are defined at the centroid of the finite volume. A representative hexahedral CV for the complex geometries, shown in Figure 2, is defined by the coordinates of the vertices which are assumed to be connected by straight lines.
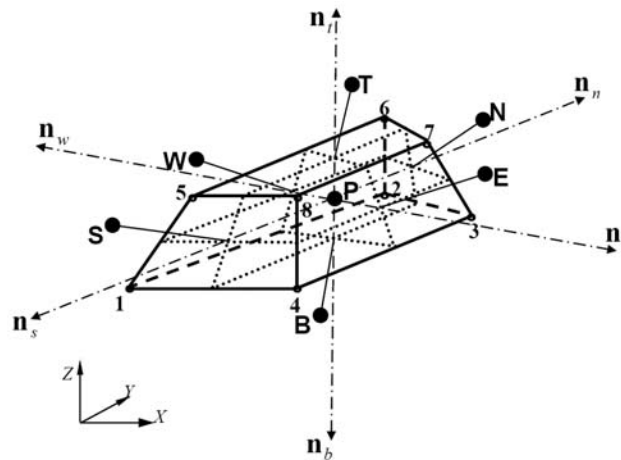
Figure 2. A representative CV

The integral equation, having infinite continuum values throughout the flow domain is discretized so as to convert into set of algebraic equations for values at centroids of the control volumes (CVs). The rate of change and source terms are integrated over the cell

volume, whereas the convection and diffusion terms are represented in terms of fluxes through the CV faces. The integral conservation equations (Eqns. (1) and (2)) are also applicable to each CV. Moreover, in the present study with Reynolds number being 400, the air flow is assumed to be incompressible therefore, Eqns. (1) and (2) take the following form:

$$\int_{\Delta S} \rho \mathbf{u} \cdot d\mathbf{S} = 0 \tag{3}$$

$$\frac{\partial}{\partial t} \int_{\Delta V_P} \rho \phi \, dV + \int_{\Delta S} \left[\rho \mathbf{u} \phi - \Gamma_\phi \nabla \phi \right] \cdot d\mathbf{S} = \int_{\Delta V_P} S_\phi \, dV \tag{4}$$

The surface integral in Eqn. (3) is discretized in the following way:

$$\int_{\Delta S} \rho \mathbf{u}.d\mathbf{S} \approx \sum_{f=e,w,n,s,t,b} \rho \left(\mathbf{u} \cdot \Delta \mathbf{S} \right)_f = \sum_f \rho \, \mathbf{u}_f \cdot \Delta \mathbf{S}_f \tag{5}$$

where $\Delta \mathbf{S}_f$ is the surface vector representing the area of the fth cell face and $\mathbf{u}_f$ is the velocity defined at the face centre f. With the definition of outward mass flux through face f, as $F_f \equiv \rho \, \mathbf{u}_f \cdot \Delta \mathbf{S}_f$, the discretized form of continuity equation (Eqn. (3)) takes the following form.

$$\sum_f F_f = F_e + F_w + F_n + F_s + F_t + F_b = 0 \tag{6}$$

The rate of change term in Eqn. (4) is a volume integral, which requires integration over the volume of the CV with approximation. The approximation is of second-order to replace for volume integral by the product of the mean value for the integrand and the volume, where the mean value for the integrand is approximated by the values at the CV centre. In general, for any value of Q over CV the approximation can be written as

$$\int_{\Delta V_P} Q \, dV = \bar{Q} \Delta V_P \approx Q_P \Delta V_P \tag{7}$$

where Q_P is the value of Q at CV centre. Eqn. (7) becomes exact if Q is either constant or varies linearly within CV; otherwise, it contains a second-order error. Using this approximation (Eqn. (7)), the rate of change term in Eqn. (4) can be discretized as follows:

$$\frac{\partial}{\partial t} \int_{\Delta V_P} \rho \phi \, dV \approx \frac{\left(\rho \phi \, dV \right)_P^{n+1} - \left(\rho \phi \, dV \right)_P^n}{\Delta t} = \rho \Delta V_P \frac{\phi_P^{n+1} - \phi_P^n}{\Delta t} \tag{8}$$

The convection flux component of variable ϕ can be approximated in the following form:

$$\int_{\Delta S} \rho \mathbf{u} \phi \cdot d\mathbf{S} \approx \sum_f \rho \phi_f \left(\mathbf{u} \cdot \Delta \mathbf{S} \right)_f = \sum_{f=e,w,n,s,t,b} F_f \phi_f \equiv F_P^c \tag{9}$$

where F_P^c represents the sum of convective fluxes ($\equiv F_f \phi_f$) over all faces of the CV. QUICK (Quadratic Upwind Interpolation for Convective Kinematics) scheme of Leonard [13] which, involves one downstream and two upstream cell centre values is used to determine the value of the convective variable (ϕ_f) at the centre of each CV face. This interpolation is dictated by the direction of mass flux at the interface F_f. If the mass flux is positive on the east face of the shaded CV shown in Figure 3 the cells with node E, P and W are the downstream, upstream and far-upstream neighbours, respectively. Otherwise if $F_f < 0$, on the east face of the CV, the respective neighbours are the cells with node P, E and EE (the east cell of cell E). The neighbours can be similarly classified for the other faces of CV. QUICK scheme uses ϕ_D, ϕ_U and ϕ_{UU} to find the face value ϕ_f as follows.

$$\phi_f = \frac{\Delta V_U \left(2\Delta V_U + \Delta V_{UU}\right)}{\left(\Delta V_D + \Delta V_U\right)\left(\Delta V_D + 2\Delta V_U + \Delta V_{UU}\right)}\phi_D + \frac{\Delta V_D \left(2\Delta V_U + \Delta V_{UU}\right)}{\left(\Delta V_D + \Delta V_U\right)\left(\Delta V_U + \Delta V_{UU}\right)}\phi_U$$
$$- \frac{\Delta V_D \, \Delta V_U}{\left(\Delta V_U + \Delta V_{UU}\right)\left(\Delta V_D + 2\Delta V_U + \Delta V_{UU}\right)}\phi_{UU} \tag{10}$$

$$F_f\phi_f = F_f \frac{\Delta V_U \left(2\Delta V_U + \Delta V_{UU}\right)}{\left(\Delta V_D + \Delta V_U\right)\left(\Delta V_D + 2\Delta V_U + \Delta V_{UU}\right)}\phi_D + F_f \frac{\Delta V_D \left(2\Delta V_U + \Delta V_{UU}\right)}{\left(\Delta V_D + \Delta V_U\right)\left(\Delta V_U + \Delta V_{UU}\right)}\phi_U$$
$$- F_f \frac{\Delta V_D \, \Delta V_U}{\left(\Delta V_U + \Delta V_{UU}\right)\left(\Delta V_D + 2\Delta V_U + \Delta V_{UU}\right)}\phi_{UU} \tag{11}$$

where ΔV_D, ΔV_U and ΔV_{UU} are the volume of the downstream, upstream and far-upstream CVs respectively.
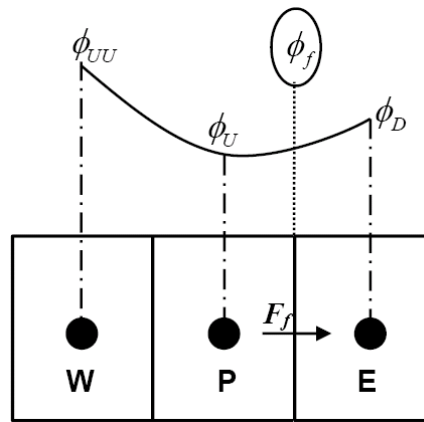
Figure 3. Schematic of the geometric interpolation/ extrapolation employed by QUICK scheme

The diffusive flux of the variable ϕ through the faces of the CV can be evaluated using ϕ as follows

$$\int_{\Delta \mathbf{S}} \Gamma_\phi \nabla \phi \cdot d\mathbf{S} \approx \sum_{f=e,w,n,s,t,b} \left(\Gamma_\phi \nabla \phi \cdot \Delta \mathbf{S}\right)_f \equiv F_P^d \tag{12}$$

For any face it can be written as

$$\Delta \mathbf{S}_f = \alpha_1 \mathbf{n}_1 + \alpha_2 \mathbf{n}_2 + \alpha_3 \mathbf{n}_3 \tag{13}$$

where $\mathbf{n}_1$, $\mathbf{n}_2$ and $\mathbf{n}_3$ are any three linearly independent unit vectors. Therefore,

$$\nabla \phi \cdot \Delta \mathbf{S}_f = \nabla \phi \cdot \left(\alpha_1 \mathbf{n}_1 + \alpha_2 \mathbf{n}_2 + \alpha_3 \mathbf{n}_3\right)$$
$$= \alpha_1 \nabla \phi \cdot \mathbf{n}_1 + \alpha_2 \nabla \phi \cdot \mathbf{n}_2 + \alpha_3 \nabla \phi \cdot \mathbf{n}_3 \tag{14}$$

If $\Delta\phi_1$, $\Delta\phi_2$ and $\Delta\phi_3$ are the difference in ϕ between the two ends of the line segments Δx_1, Δx_2 and Δx_3 then

$$\Delta\phi_1 = \nabla \phi \cdot \Delta \mathbf{x}_1, \quad \Delta\phi_2 = \nabla \phi \cdot \Delta \mathbf{x}_2, \quad \Delta\phi_3 = \nabla \phi \cdot \Delta \mathbf{x}_3 \tag{15}$$

where $\Delta \mathbf{x}_1$, $\Delta \mathbf{x}_2$ and $\Delta \mathbf{x}_3$ are the vectors associated with Δx_1, Δx_2 and Δx_3, respectively. If $\Delta \mathbf{x}_1$, $\Delta \mathbf{x}_2$ and $\Delta \mathbf{x}_3$ are in the directions of $\mathbf{n}_1$, $\mathbf{n}_2$ and $\mathbf{n}_3$ respectively, then it follows from Eqn. (15) that

$$\frac{\Delta\phi_1}{\Delta x_1} = \nabla \phi \cdot \mathbf{n}_1, \quad \frac{\Delta\phi_2}{\Delta x_2} = \nabla \phi \cdot \mathbf{n}_2, \quad \frac{\Delta\phi_3}{\Delta x_3} = \nabla \phi \cdot \mathbf{n}_3 \tag{16}$$

where Δx_1, Δx_2 and Δx_3 are the magnitudes of $\Delta \mathbf{x}_1$, $\Delta \mathbf{x}_2$ and $\Delta \mathbf{x}_3$. Consequently, using Eqns. (15) and (16) it can be written as

$$\nabla \phi \cdot \Delta \mathbf{S}_f = \alpha_1 \frac{\Delta \phi_1}{\Delta x_1} + \alpha_2 \frac{\Delta \phi_2}{\Delta x_2} + \alpha_3 \frac{\Delta \phi_3}{\Delta x_3} \tag{17}$$

To get α_1, α_2 and α_3, the unit vectors are expressed as $\mathbf{n}_1 = \left(n_{11} \ n_{12} \ n_{13} \right)$, $\mathbf{n}_2 = \left(n_{21} \ n_{22} \ n_{23} \right)$ and $\mathbf{n}_3 = \left(n_{31} \ n_{32} \ n_{33} \right)$, where n_{11}, n_{12} and n_{13} are the Cartesian components of $\mathbf{n}_1$ and is determined by $\frac{\Delta x_{11}}{\Delta x_1}$, $\frac{\Delta x_{12}}{\Delta x_1}$ and $\frac{\Delta x_{13}}{\Delta x_1}$, where Δx_{11}, Δx_{12} and Δx_{13} are the three components of vector $\Delta \mathbf{x}_1$. The other values n_{21}, n_{22} ..., n_{33} etc. can be similarly determined. Therefore Eqn. (13) can be written as $\begin{bmatrix} n_{11} \ n_{12} \ n_{13} \\ n_{21} \ n_{22} \ n_{23} \\ n_{31} \ n_{32} \ n_{33} \end{bmatrix}^T \begin{Bmatrix} \alpha_1 \\ \alpha_2 \\ \alpha_3 \end{Bmatrix} = \begin{Bmatrix} \Delta S_{1f} \\ \Delta S_{2f} \\ \Delta S_{3f} \end{Bmatrix}$, where S_{1f}, S_{2f}, S_{3f} are the Cartesian components of the surface vector S_f. The values α_1, α_2 and α_3 are determined using Cramer's rule, $\alpha_1 = \frac{D_1}{D}$, $\alpha_2 = \frac{D_2}{D}$ and $\alpha_3 = \frac{D_3}{D}$, where D is the determinant of the coefficient matrix, and D_1 is obtained by replacing the first column of D by the column with elements S_{1f}, S_{2f}, S_{3f} and so on.

The east face is taken to illustrate the diffusion model. It is shown in Figure 4. Given the edge centre values ϕ_{te}, ϕ_{be}, ϕ_{se}, ϕ_{ne}, the diffusion flux is computed as follows.

$$F_P^d = \Gamma_\phi \left(\alpha_1 \frac{\phi_E - \phi_P}{\Delta x_1} + \alpha_2 \frac{\phi_{ne} - \phi_{se}}{\Delta x_2} + \alpha_3 \frac{\phi_{te} - \phi_{be}}{\Delta x_3} \right) \tag{18}$$
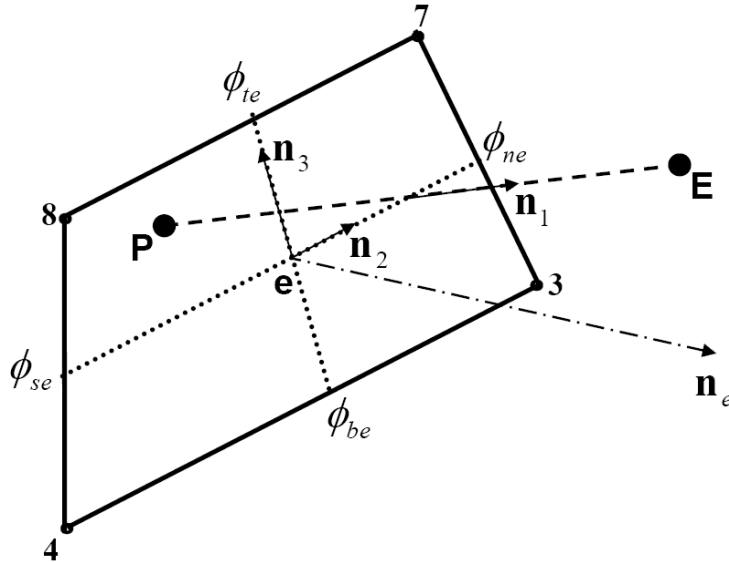
Figure 4. East face representation

To calculate the edge centre values appearing in cross-derivative diffusion flux, the following interpolation scheme is used.

$$\phi_{te} = \frac{\Delta V_{TE}\, \phi_P + \Delta V_P\, \phi_{TE} + \Delta V_T\, \phi_E + \Delta V_E\, \phi_T}{\Delta V_{TE} + \Delta V_P + \Delta V_T + \Delta V_E} \tag{19a}$$

$$\phi_{be} = \frac{\Delta V_{BE}\, \phi_P + \Delta V_P\, \phi_{BE} + \Delta V_B\, \phi_E + \Delta V_E\, \phi_B}{\Delta V_{BE} + \Delta V_P + \Delta V_B + \Delta V_E} \tag{19b}$$

$$\phi_{ne} = \frac{\Delta V_{NE}\, \phi_P + \Delta V_P\, \phi_{NE} + \Delta V_N\, \phi_E + \Delta V_E\, \phi_N}{\Delta V_{NE} + \Delta V_P + \Delta V_N + \Delta V_E} \tag{19c}$$

$$\phi_{se} = \frac{\Delta V_{SE}\, \phi_P + \Delta V_P\, \phi_{SE} + \Delta V_S\, \phi_E + \Delta V_E\, \phi_S}{\Delta V_{SE} + \Delta V_P + \Delta V_S + \Delta V_E} \tag{19d}$$

where V_{TE} is the volume of the top-east neighbouring cell to the cell P, and ϕ_{te} is the edge centre value of the top-east edge. Other edge centres can be similarly interpolated.

The source term is to be integrated over the cell volume. By applying the volume integral approximation (Eqn. (7)), i.e., assuming that the specific source at the CV centre represents the mean value over the whole control volume, it can be written as

$$\int_{\Delta V_P} S_\phi\, dV \approx \left(S_\phi\right)_P \Delta V_P \tag{20}$$

The pressure term in the momentum equation is also included as a source term. Its discretizaion is analogous to that of the ordinary diffusion flux, i.e., for the momentum equation for the velocity component u_i (= u, v, w, respectively), the pressure term is

$$-\int_{\Delta V_P} \nabla p \cdot \mathbf{n}_i\, dV \approx -\left(\nabla p \cdot \mathbf{n}_i\right)_P \Delta V_P \tag{21}$$

where $\mathbf{n}_i$ is the unit vector in the direction of the velocity component, u_i. However, the Gauss divergence theorem can be used to convert the volume integral to a surface integral which can be discretized as

$$-\int_{\Delta S} p\, \mathbf{n}_i\, d\mathbf{S} \approx -\sum_{f=e,w,n,s,t,b} p_f\, \Delta S_{if} \tag{22}$$

where p_f is the pressure at the fth face centre and ΔS_{if} is the ith direction component of the surface vector for face f.

3.3. Boundary conditions:

The boundaries of the computational domain fall under four categories, inlet, exit, symmetrical side-walls, and no-slip isothermal solid surfaces. The boundary conditions have been summarized in Table-1.

TABLE1: BOUNDARY CONDITIONS

• Top and bottom walls: $u = v = w = 0$, $\dfrac{\partial p}{\partial z} = 0$ and $T = T_W$
• Side walls: $\dfrac{\partial u}{\partial y} = \dfrac{\partial w}{\partial y} = 0$, $v = 0$, $\dfrac{\partial p}{\partial y} = 0$ and $\dfrac{\partial T}{\partial y} = 0$
• Inlet to the channel: $u = U_\infty$, $v = w = 0$, $\dfrac{\partial p}{\partial x} = 0$ and $T = T_\infty$
• Channel exit: $\dfrac{\partial \phi}{\partial t} + U_{av}\dfrac{\partial \phi}{\partial x} = 0$; Orlanski, [14]
• Obstacle surfaces (tube surface): $u = v = w = 0$, $\dfrac{\partial p}{\partial n} = 0$ and $T = T_W$; where n denotes normal to the surface

3.4. Solution methodology:

A pressure-based method on a collocated grid arrangement for steady and unsteady flows was developed by Darbandi and Vakilipour [15]. They estimated the advection terms on the cell faces using an inclusive pressure-weighted up-winding scheme extended on unstructured grids. However, to avoid a non-physical spurious pressure field pattern, two mass fluxes per volume expressions were employed at the cell interfaces. They compared their results based on finite-volume and finite-element methods. Semi-explicit method has been used in the present to solve the discretized equations. The discretized form of the momentum equation for the ith velocity component u_i, viz.

$$\rho \Delta V_P \frac{u_{iP}^{n+1} - u_{iP}^n}{\Delta t} + \left(F_e^c + F_e^d \right)^n = -\sum_f p_f^{n+1} \Delta S_{if} \tag{23}$$

has been solved with

$$\sum_f F_f^{n+1} = 0 \tag{24}$$

made satisfied for each finite volume cell. However, due to the non-staggered variable arrangement, if the variables (velocity and pressure) at the cell faces are calculated by linear interpolation between the adjacent cell centred quantities then the pressure velocity iterations do not converge and lead to a checker board pressure field. Therefore, it is important to use momentum interpolation (Rhie and Chow, [16]; Majumdar *et al.*, [17]) in which the velocity at all the cell faces are computed by allowing linear interpolation of the convective and diffusive terms but not of the pressure term. The velocity and pressure fields are calculated using Gauss-Seidel type algorithm (Eswaran and Prakash, [18]). The discretization procedure and the solution methodology used in the present study is also documented in Muralidhar and Sundararajan [19].

4. Results and discussion

Figures 5 and 6 present the instantaneous streamlines near the bottom wall of the channel and in the cross-stream plane located at a distance of 2D downstream from centre of the circular tube for the case of single and at the distance of 2D from downstream tube for the inline arrangement of two tubes respectively. Various time instants considered are with respect to separation of the shear layer from the lower surface of the tube. Apparently, the growth of the asymmetric vortex bubble formed due to wrapping of the lower shear layer is observed. The corresponding adjacent streamlines in the cross-stream plane indicate the evolution of the other alternating vortex pair. The streamlines in the cross-stream plane show asymmetry about the mid-vertical as well as mid-horizontal planes. This is obviously due to planar vortex shedding in the wake and also due to three-dimensional nature of the confined flow between channel walls.

Figures 7(a) and 7(b) present the vorticity field at different time steps for the two cases considered. For the considered Reynolds number, even though the flow is laminar, the asymmetry in the wake is apparent from the vorticity contour. For the inline arrangement of tubes, the vorticity contour in the wake of the downstream tube shows qualitative differences with respect to that in the wake of the upstream tube mainly due to difference in the nature of the flow that impinges upon them. Moreover, the vertical structure in the wake of the upstream tube is similar to that in the wake for flow past single tube except that it gets obstructed due to presence of the downstream tube.
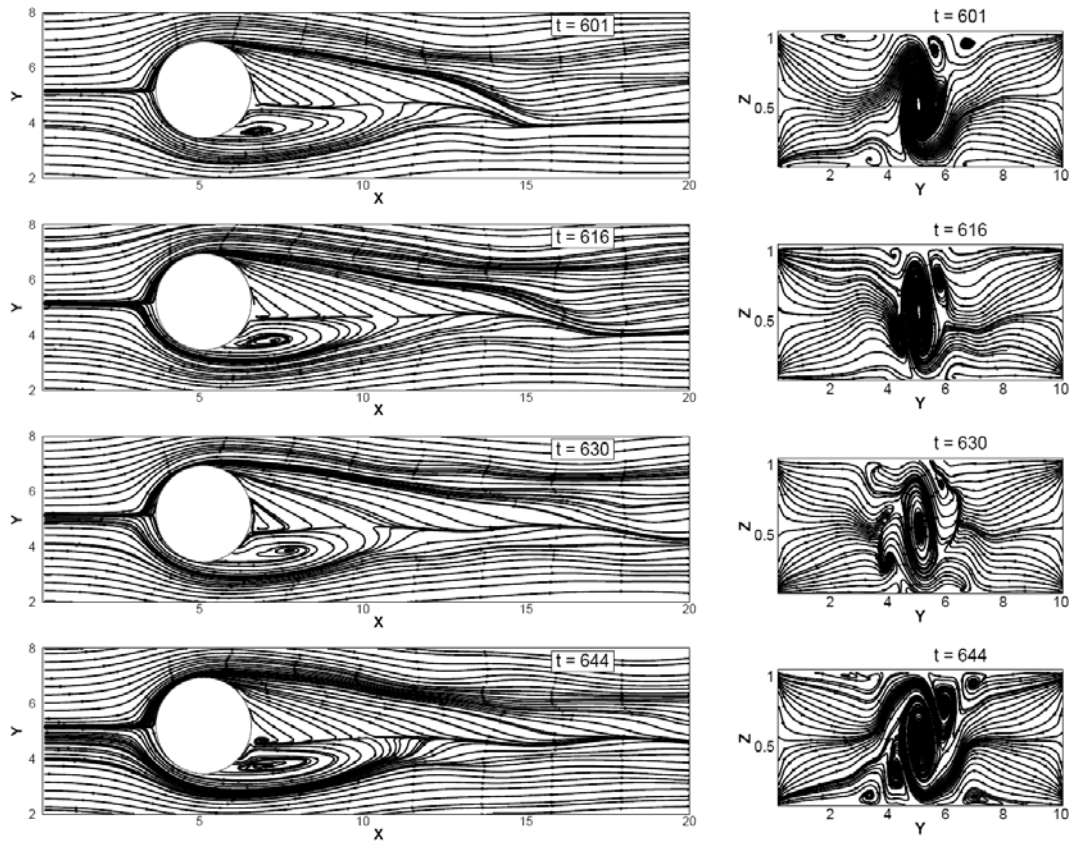
Figure 5. Instantaneous streamline plots at different time steps for single tube
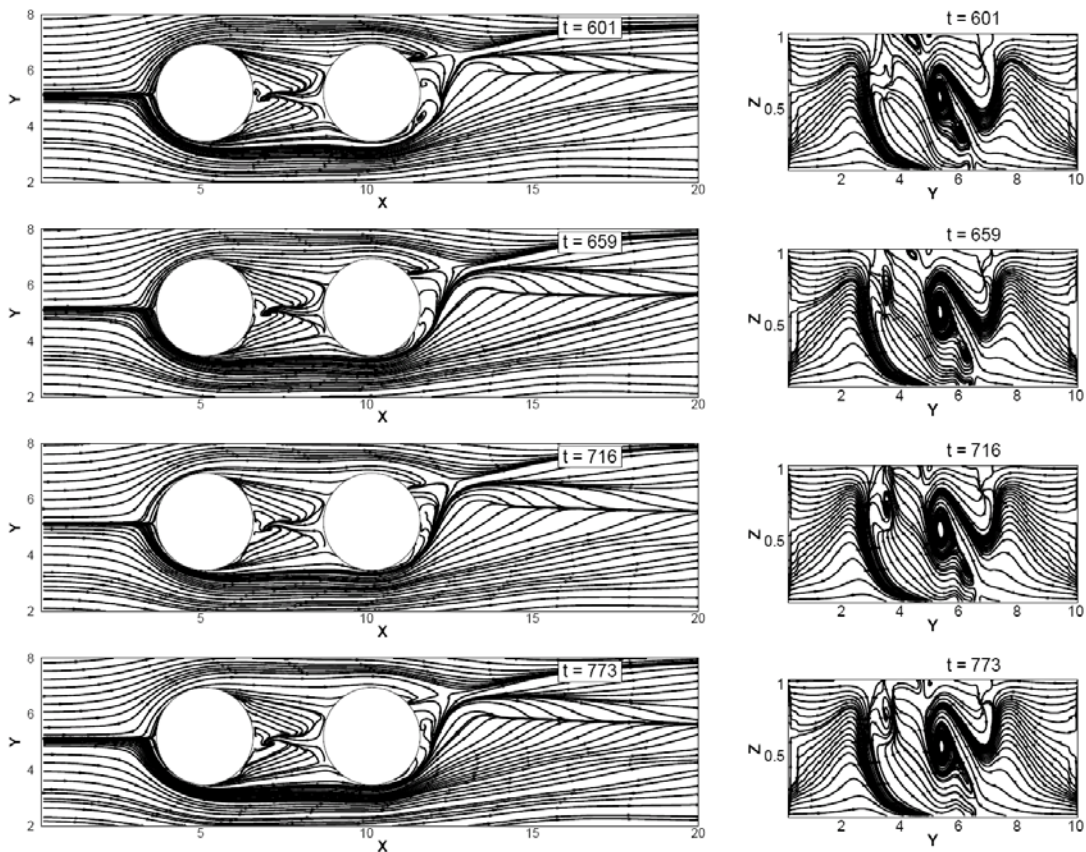
Figure 6. Instantaneous streamline plots at different time steps for two inline tubes
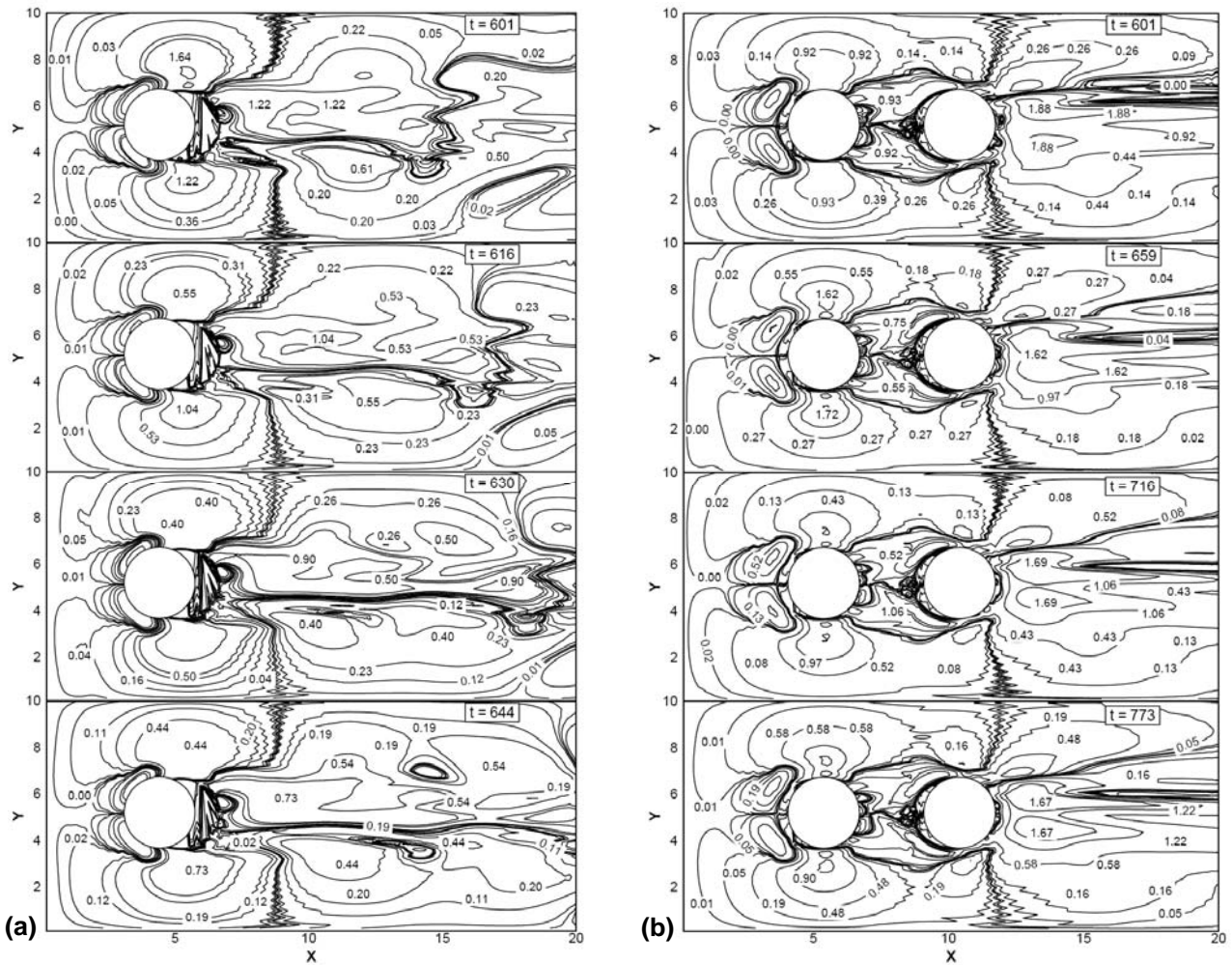
Figure 7. Instantaneous vorticity field at different time steps (a) single tube (b) two inline tubes

The instantaneous temperature contours near the bottom wall of the channel are shown in Figures 9(a) and 9(b) for single and two inline arrangements of tube, respectively. A higher temperature in the wake region indicates zone of poor heat transfer. At certain instant of time, the wake may show poor transport characteristics and higher temperature while at other time the transport may improve and local temperature in the wake region may become smaller. Incidentally, for single tube case at t = 601, when the lower vortex bubble is smaller in size, the wake is almost under the influence of upper enveloping shear layer which has wrapped up to such an extent that the wake becomes nearly stagnant giving rise to higher local temperature in the region. At other instants of time, the mean wake temperature decreases due to improved fluid transport.

Figures 8(a) and 8(b) show the variation of span-averaged pressure along length of the channel at different time instants. In fact, over one time period of vortex shedding, the pressure variation can be better represented by the span-averaged pressure of the time-averaged field. This temporal evolution of the pressure field indicates that even though due to oscillating shear layers, the wake pressure fluctuates with time, the overall pressure drop across the channel does not get affected. This nature has been confirmed for the inline arrangement of two tubes as well.

For flow past inline arrangement of two circular tubes, the front stagnation line of the downstream tube is 3H behind the rear stagnation line of the upstream tube. Such a small separation between the two tubes affects the unsteady wake zone behind the upstream tube that vortex shedding in its wake gets almost suppressed (flow field not being shown due to lack of space). This is apparent from the temperature contours in the wake region of the upstream tube. On the other

hand, the wake of the downstream tube demonstrates vortex shedding which differs in nature when compared to wake of single tube in free stream. However, the qualitatively nature of the unsteady flow in the wake of the downstream tube can be well interpreted from the asymmetric temperature contours. The temperature contours shown do not correspond to exactly same time instants shown in Figure 9(a) for flow past single circular tube.

(a)   (b)
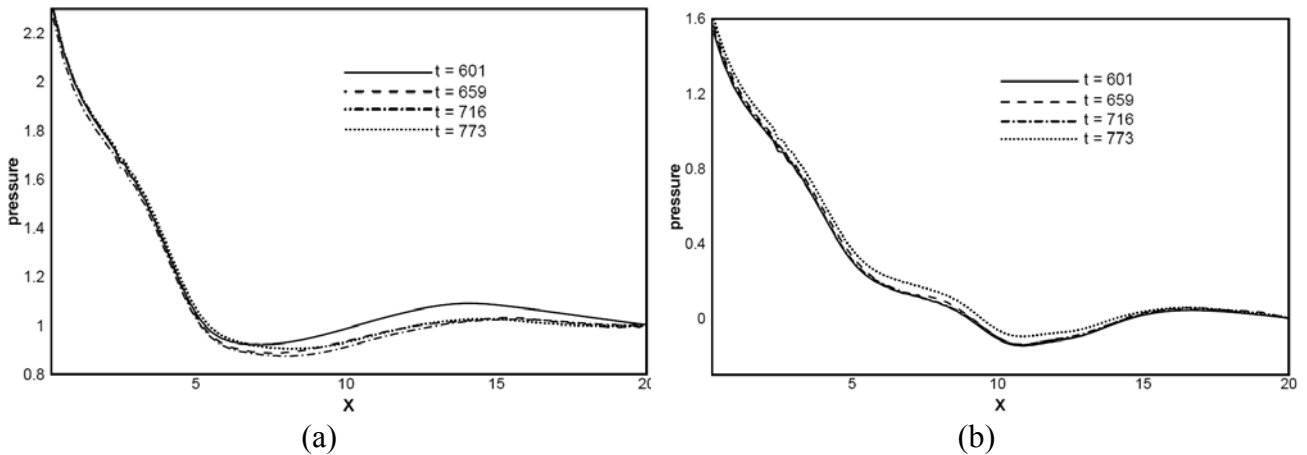
Figure 8. Instantaneous pressure at different time steps (a) single tube (b) two inline tubes

(a)   (b)
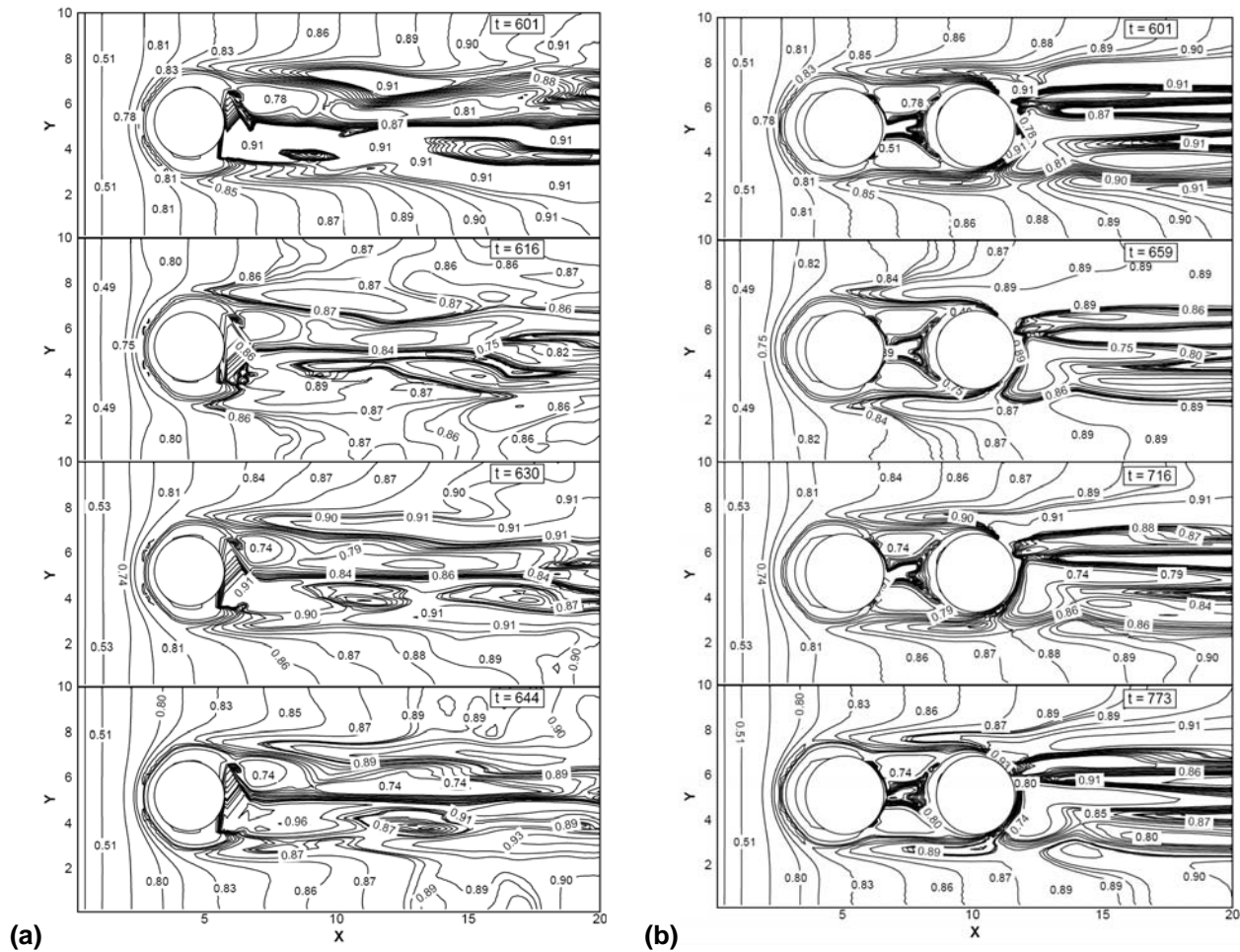
Figure 9. Instantaneous temperature distribution at different time steps
(a) single tube (b) two inline tubes
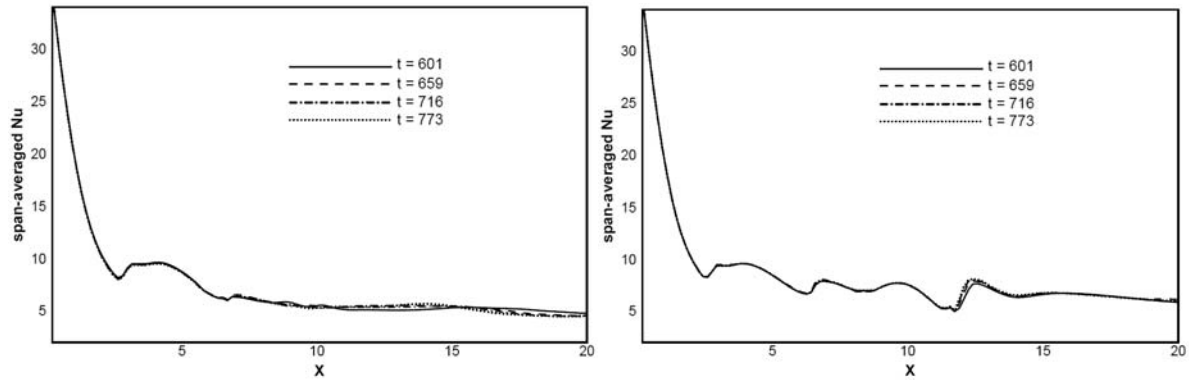
Figure 10. Instantaneous Span-averaged Nusselt number
(a) single tube (b) two inline tubes

Figures 10(a) and 10(b) show the variation of span-averaged Nusselt number near the bottom channel wall along length of the channel at the four time instants chosen for temperature contours in Figures 8(a) and 8(b). The Nusselt number is based on bulk-mean temperature of the fluid in the local cross-stream plane. It is seen that due to arrested wake of the upstream tube in presence of the downstream tube, the span-averaged Nusselt number in its wake remains almost constant. Even in the wake of the downstream tube, the temporal variation of span-averaged Nusselt number is not significant. However, the variation of local Nusselt number near channel walls, at a particular spanwise location, shows appreciable temporal dependence.

5. Conclusion

Three-dimensional computations have been carried out using finite volume-based developed computational code to study the flow and heat transfer characteristics in the unsteady wake of a channel confined single circular tube and an inline arrangement of two circular tubes. Temporal evolution of flow and temperature fields, span-averaged pressure and span-averaged Nusselt variation along length of the channel has been presented. The otherwise unsteady wake of a single circular tube shows nearly steady flow and thermal characteristics in presence of a downstream tube. Moreover, the unsteady flow and temperature fields in the wake of a circular tube placed in free stream differ significantly from those in the wake of a tube placed in the wake of another upstream tube. From this study it can be concluded that for comparison of overall flow and heat transfer characteristics of various tube arrangements, it is worthwhile to consider time-averaged flow and temperature fields over a fixed interval of time. Even though the time-averaged fields do not exactly correspond to any of the particular instantaneous filed, time-averaged fields display overall flow characteristics.

Nomenclature

A	area
CV	control volume
D	diameter of circular tube
$\vec{F}$	flux vector
f	face of CV
H	channel height ($= l_3$)
l	length
Nu	Nusselt number

$\overline{\overline{Nu}}$	average Nusselt number
n	normal to surface
p	pressure
$\bar{p}$	span-averaged and height-averaged pressure
S_ϕ	volumetric source term
Re_D	Reynolds number based on tube diameter $\left(=VD/\upsilon\right)$
S	surface vetor
T	temperature
t	time
V	Volume of CV
u	axial velocity component
v	span-wise velocity component
w	velocity component normal to channel wall

Greek

Δ	difference/ increment
Γ	diffusion coefficient
μ	dynamic viscosity
ν	kinematic viscosity
ϕ	transport property (u, v, w or T)
ρ	density
θ	angle measured clockwise from forward stagnation point with respect to tube center

Subscript

1	span-wise direction
2	transverse direction
3	direction normal to channel wall
$c1$	centre of upstream tube from the channel inlet
e	east
n	north
s	south
w	west

References

[1]   Tiwari Shaligram, Pratish P. Patil, Jayavel S., and Biswas G. Flow field characteristics near first transition for flow past a circular tube confined in a narrow channel. in 2006 Proceedings of the 33rd National & 3rd International Fluid Mechanics and Fluid Power Conference, NCFMFP2006-1132. IIT Bombay, India.

[2]   Pratish P. Patil, and Tiwari Shaligram, Numerical investigation of laminar unsteady wakes behind two inline square cylinders confined in a channel. Engineering Application of Computational Fluid Mechanics, 2009. 3: p. 369-386.

[3]   Wilson Safwat A., and Khalil Bassiouny M. Modeling of heat transfer for flow across tube banks. Chemical Engineering and Processing, 2000. 39: p. 1-14.

[4]   Baker C.J. Oscillations of horseshoe vortex systems. ASME Journal of Fluids Engineering, 1991 113(3): p. 489-495.

[5]   Roychowdhury Ghosh D., Sarit Kumar Das, and Sundararajan T. Numerical simulation of laminar flow and heat transfer over banks of staggered cylinders. International Journal of Numerical Methods in Fluids, 2002. 39: p. 23-40.

[6]   Nishimura Tatsuo, Hisayoshi Itoh, Hisashi Miyashita, The influence of tube layout on flow and mass transfer characteristics in tube banks in the transitional flow regime. International Journal of Heat and Mass Transfer, 1993. 36(3): p. 553-563.

[7]   Williamson, C.H.K. Vortex dynamics in the cylinder wake. Annual Review of Fluid Mechanics, 1996. 28: p. 477–539.

[8]   Zdravkovich, M.M. Flow Around Circular Cylinders. Vol. 1, Oxford University Press. Oxford. 1997.

[9]   Ju Lili, and Du Qiang, A finite volume method on general surfaces and its error estimates. Journal of Mathematical Analysis and Applications, 2009. 352: p. 645-668.

[10]   Piller, M, and Stalio, E. Compact finite volume schemes on boundary-fitted grids. Journal of Computational Physics, 2008. 227: p. 4736-4762.

[11]   Lacor Chris, Sergey Smirnov, and Martine Baelmans, A finite volume formulation of compact central schemes on arbitrary structured grids. Journal of Computational Physics, 2004. 198: p. 535-566.

[12]   Pereira, J.M.C, Kobayashi, M.H., and Pereira, J.C.F. A fourth-order-accurate finite volume compact method for the incompressible Navier–Stokes solutions. Journal of Computational Physics, 2001. 167: p. 217-243.

[13]   Leonard, B.P. A stable and accurate convective modeling procedure based on quadratic upstream interpolation. Computational Methods in Applied Mechanics Engineering, 1979. 19: p. 59-98.

[14]   Orlanski, I. A simple boundary condition for unbounded flows. Journal of Computational Physics, 1976. 21: p. 251-269.

[15]   Darbandi, M., and Vakilipour, S. Developing implicit pressure-weighted upwinding scheme to calculate steady and unsteady flows on unstructured grids. International Journal for Numerical Methods in Fluids, 2008. 56: pp. 115-141.

[16]   Eswaran, V., and Prakash, S. A finite volume method for Navier-Stokes equations. in 1998 Proceedings of the Third Asian CFD Conference, 1: p. 251-269, Bangalore, India.

[17]   Rhie, C. M., and Chow, W. L., Numerical study of the turbulent flow past an airfoil with trailing separation. AIAA Journal, 1983. 2: p. 1525-1532.

[18]   Majumdar, S., Rodi, W., and Zhu, J., Three-dimensional finite volume method for incompressible flows with complex boundaries. Journal of Fluids Engineering (ASME), 1992. 114: p. 496-503.

[19]   Muralidhar, K., and Sundararajan, T., Computational Fluid Flow and Heat Transfer. (Chapter: 12 – The Finite Volume Method by Atul Sharma, and Vinayak Eswaran), 2005. 2nd Ed., Narosa Publishing House, India.